

# Optimal Capping Layer Thickness for Stacked Quantum Dots

X.B. Niu<sup>1</sup>, Y-J Lee<sup>2</sup>, R.E. Caflisch<sup>1,2</sup>, and C. Ratsch<sup>2,3</sup>

<sup>1</sup>*Department of Material Sciences and Engineering, UCLA, Los Angeles, CA 90095*

<sup>2</sup>*Department of Mathematics, UCLA, Los Angeles, CA 90095*

<sup>3</sup>*Institute for Pure and Applied Mathematics, UCLA, Los Angeles, CA 90095*

We study the effect of strain on the vertical and lateral self-organization of nanoscale patterns and stacked quantum dots during epitaxial growth. The computational approach is based on the level set method in combination with an atomistic strain code. Strain changes the energetics of microscopic parameters during growth, and thus determines the nucleation sites and the growth of islands and dots. Our results show that strain can lead to vertical alignment as well as lateral organization. Moreover, our simulations suggest that there is an optimal thickness of the capping layer to get the best alignment and most uniform size distribution of stacked quantum dots, and that its variation can be used to control the formation of interesting structures.

Material systems with highly ordered and uniformly sized nanoscale patterns and stacked quantum dots (QDs) hold great promise for many technological applications. QDs for semiconductor systems open the door to the next generation of opto-electronic devices [1, 2]. Ordered nanoscale patterns and stacked QDs in metallic systems can be used for storage devices [3] or nanocatalysis [4]. A common approach to synthesizing nanoscale patterns and QDs is through vacuum deposition techniques, where the desired structures grow epitaxially on a substrate. Critical factors for the performance of all such devices are the degree of uniformity in size and spacing of nano patterns and QDs. Therefore, there has been a tremendous interest in understanding the formation and growth of nanoscale patterns and stacked QDs [5, 6] and controlling their size distribution.

It has been observed for semiconductor systems that kinetic and/or thermodynamic factors that result from strain due to a lattice mismatch spontaneously lead to the formation of QDs [7–9]. Moreover, under the right conditions, these QDs are ordered laterally [10] or vertically [11, 12]. It would therefore be very desirable to control and tune this ordering. Buried islands, QDs or defects introduce a long-range strain field, which is believed to alter the kinetic and thermodynamic driving forces during growth. Strain induced variations of the chemical potential have been suggested to be the driving force for vertical ordering in previous simple models [13–15]. In these models islands form because of *thermodynamic* arguments, where the chemical potential is low. But neither of these models have considered the effect of strain on the *kinetic* parameters that govern diffusion and nucleation.

In this letter, we demonstrate that strain due to a lattice mismatch can lead to lateral organization and vertical alignment (or anti-alignment) of nanoscale patterns and stacked QDs because it modifies the potential energy surface (PES) for surface diffusion. Kinetic and thermodynamic driving forces are included within the same theoretical framework. We show that self-organization of stacked QDs can be obtained by kinetic as well as ther-

modynamic effects. We find that the thickness of the capping layer during growth of stacked QDs affects the strain in the system, and thus the PES for surface diffusion. Our results suggest that there is an optimal thickness of the capping layer that leads to the best ordering of stacked QDs.

We model epitaxial growth using the level set (LS) approach to epitaxial phenomena [16–18]. In this model, islands are resolved as atomistic in height but continuous in the lateral dimensions. We use dimensionless atomic units. Adatoms are represented by an adatom density  $\rho(\mathbf{x}, t)$ , which is updated by solving the following diffusion equation:

$$\frac{\partial \rho}{\partial t} = F + \nabla \cdot (\mathbf{D} \nabla \rho) - 2 \frac{dN}{dt} + \nabla \cdot \left( \frac{\rho}{k_B T} \mathbf{D} \nabla E_{\text{ad}} \right) \quad . \quad (1)$$

In eq. (1),  $\mathbf{D}$  is a diffusion tensor where the diagonal entries are labeled  $D_i(\mathbf{x})$  and  $D_j(\mathbf{x})$ , and correspond to diffusion along the two directions  $i$  and  $j$ . For simplicity no other direction for diffusion is included (but could easily be incorporated).  $F$  is the deposition flux,  $dN/dt$  is the nucleation rate, and the last term is the thermodynamic drift.  $E_{\text{ad}}$  is the adsorption energy (see below). We enforce a boundary condition  $\rho(\mathbf{x}) = \rho_{\text{eq}}(D_{\text{det}}(\mathbf{x}), \mathbf{x})$ , where  $D_{\text{det}}(\mathbf{x})$  is a (spatially varying) detachment rate [19]. The gradient of  $\rho$  at the boundary then determines the growth of the islands [16–18]. The nucleation rate is given by [17]

$$dN/dt = \sigma_1 \langle [(D_i(\mathbf{x}) + D_j(\mathbf{x}))/2] \rho^2(\mathbf{x}) \rangle \quad , \quad (2)$$

where  $\sigma_1$  is the so-called capture number [20], and the average  $\langle \cdot \rangle$  is taken over all lattice sites.

The rates for adatom diffusion  $D_i(\mathbf{x})$  and  $D_j(\mathbf{x})$  are determined by an expression of the form  $D = D_0 \exp(-\Delta E/k_B T)$ , where  $D_0$  is a prefactor (chosen to be  $10^{13} \text{s}^{-1}$ ),  $k_B$  is the Boltzman constant,  $T$  is the temperature, and  $\Delta E$  is the energy barrier for surface diffusion, given by  $\Delta E = E_{\text{trans}} - E_{\text{ad}}$ . The parameters  $E_{\text{trans}}$  and  $E_{\text{ad}}$  refer to the transition energy and adsorption (or binding) energy for an adatom that might diffuse. Our approach allows for a spatially varying PES for surface

diffusion, or more precisely, for spatial variation of  $E_{\text{trans}}$  and  $E_{\text{ad}}$  (that is determined by the local strain) [18]. Therefore the diffusion constants  $D_i(\mathbf{x})$  and  $D_j(\mathbf{x})$  and the thermodynamic drift are also spatially varying.

We use an atomistic strain model that is based on harmonic potentials and includes nearest neighbor, next nearest neighbor, and bond-bending interactions [21]. It is the goal of our work to explore qualitative trends, and we therefore believe that our elastic model is adequate, and captures all the essential physics. The local strain is then calculated in our model by minimizing the discrete strain energy. We define a total strain on top of the capping layer as  $S_{\text{tot}}(\mathbf{x}) = \sqrt{(1 + S_i(\mathbf{x}))(1 + S_j(\mathbf{x}))} - 1$ , which is essentially an average of the strains in  $i$  and  $j$  direction  $S_i(\mathbf{x})$  and  $S_j(\mathbf{x})$ .

The effect of strain on  $E_{\text{trans}}$  and  $E_{\text{ad}}$  is assumed to be linear. This is in agreement with recent density function theory (DFT) calculations [22, 23] that show that  $E_{\text{trans}}$  and  $E_{\text{ad}}$  decrease with an increasing relative lattice constant (or increasing strain). For semiconductors, the diffusion barrier decreases with increasing relative lattice constant [22] (i.e.  $E_{\text{trans}}$  changes faster than  $E_{\text{ad}}$ ) and the reverse is true for metals [23]. The results presented here refer to an idealized semiconductor system with 4% misfit. We assume a diffusion barrier for the unstrained system of  $\Delta E = 833$  meV (which corresponds to  $D = 10^7$  s $^{-1}$  at  $T = 700$ K). Strain then decreases  $E_{\text{trans}}$  and  $E_{\text{ad}}$  by 250 meV and 150 meV, respectively, per 1% misfit, leading to a decrease of  $\Delta E$  by 100 meV per 1% misfit. For simplicity, we ignore surface reconstructions and their dependence upon strain [24]. We note that the results reported below are qualitatively the same for an idealized metal system, even though for metal systems the effect of strain on  $E_{\text{trans}}$  and  $E_{\text{ad}}$  is inverted.

To understand the mechanism of stacked QD growth, we first investigate the most probable nucleation sites on top of the capping layer. We consider a simple case with a single circular island of diameter 30 and height 3 in a system of size  $60 \times 60$ . The island is then covered with a capping layer of different thicknesses  $n$ , i.e., the layer has thickness  $n + 3$ . We assume that the lattice constant of the material of the island is larger than the one of the capping layer (which is the same as the substrate). Fig. 1 shows the calculated nucleation rates along the dotted line  $j = 30$  on top of the capping layer just before the first island nucleates. Clearly, the spatial variation of the nucleation rate is correlated to the position of the buried island. But the most striking result is that the most likely nucleation site moves from a position above the edge of the island to a position above the center of the island, as  $n$  increases.

The explanation for this behavior is the following: The buried island wants to assume a lattice constant that is larger than the substrate, and it relaxes most at the island edges. The material of the capping layer is therefore also expanded above the island. When  $n$  is small ( $n=0$

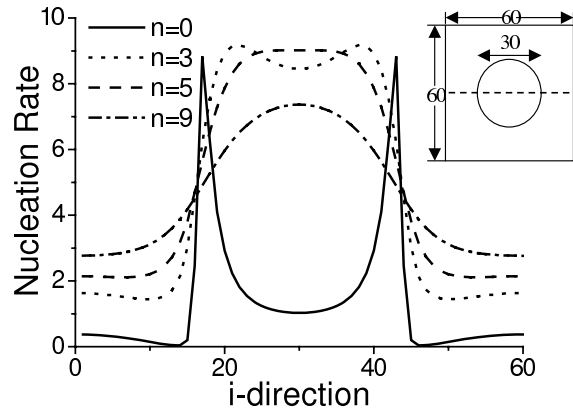


FIG. 1: Nucleation rates on top of the capping layer above a buried island with different capping layer thickness  $n$ . A schematic of the buried island is shown in the upper right corner. The nucleation rates is plotted along the dotted line  $j = 30$  in the schematic.

and  $n=3$ ), the capping layer is most expanded above the island boundary. This tensile strain leads to a lowering of  $E_{\text{ad}}$ . As a result,  $\rho$  increases (due to the thermodynamic drift), and  $D$  increases. Both effects enhance the nucleation rate [cf. eq. (2)] above the edge of the island. But as  $n$  increases to moderate values ( $n=5$ ), the lattice constant above the center of the island remains (slightly) expanded, while the lattice constant above the edges is “pushed back” to the lattice constant of the substrate and capping layer. As a result the region with largest tensile strain moves toward the center of the island. Correspondingly, the preferred nucleation site moves to the center. As  $n$  increases further ( $n=9$ ), the preferred nucleation site remains in the center, but the relative importance of the center site (with respect to sites far away) diminishes. Ultimately the system loses all memory of the buried island.

We note that the situation is more complicated for metals. Here, an increased strain lowers  $E_{\text{ad}}$  (and thus increases  $\rho$ ), but also lowers  $D$ . So the two contributions to the nucleation rate [cf. eq. (2)] behave oppositely. For typical parameters for metals the effect on the drift term dominates, and the behavior is qualitatively the same as for semiconductors. But for more extreme parameterizations for metals, or possible for cases where diffusion is dominated by more complicated events (that involve more than just one atom), it is possible that kinetic effects dominate, i.e., that the effect of strain on  $D$  is more important than the effect of  $\rho$ . For such systems, nucleation is always preferred above the island edge. It is therefore important to include kinetic effects as a possible driving force for ordering in any model, and to understand the relative importance of kinetics and thermodynamics.

To illustrate the importance of strain induced bias on the nucleation site, first consider the following, simple

case: We start with a system that is pre-patterned as shown in Fig. 2(a). The system is of size  $200 \times 200$ , with 8 circular islands of diameter 14 and height 3, along the  $i$  and  $j$  directions. The spacing along the  $j$  direction is homogeneous, while an alternating long and short spacing is imposed along the  $i$  direction, leading to a “zig-zag” pattern. The average spacing is 25, which compares very well to the spacing of about 50 nm between islands for stacked InAs islands on GaAs [11, 12], or the spacing between reconstruction lines for the observed Herringbone reconstruction of Au/Au(111) [25]. The question now is: will strain lead to an ordering of this pattern, as we grow  $N$  superlayers of stacked QDs? For computational convenience, we do not actually grow the capping layer within the growth model. Instead, we assume that the islands are capped by a (perfectly smooth) capping layer of a fixed thickness  $n$ . But before growing the next set of islands we properly calculate the entire strain field on top of the new capping layer (and above the buried islands). Islands are then nucleated and grown according to the strain induced variations of the PES. Based on the experimental size and height of QDs [11, 12], we grow the islands to 20% monolayer. For computational convenience we then manually increase the height to 3 and add a perfectly smooth capping layer. The procedure is then repeated  $N$  times.

Figs. 2 (b), (c), and (d) show a top view of the morphology after  $N = 40$  superlayers have been grown with different capping layer thicknesses  $n$ . Figs. 2 (e), (f), and (g), show a corresponding side view, that can be compared to a cross-sectional transmission electron microscopy (TEM) image. It is immediately evident that for the intermediate value  $n = 2$  islands nicely align on top of each other [Figs. 2 (c) and (f)]. The pre-imposed “zig-zag” structure disappears, and islands form a regular pattern. The reason is that islands nucleate above the center of the islands underneath. Then, islands grow preferentially toward the longer gap between the adjacent islands. Gradually, the island positions shift slightly, leading ultimately to the near perfect ordering. In contrast, when  $n$  is too small, islands nucleate above the edge of the islands underneath, and we never get the nice spatial ordering. This can be seen in Figs. 2 (b) and (e). When  $n = 4$  [cf. Figs. 2 (d) and (g)], there is not a nucleation above every previous island. Fluctuations and more defects lead to a worsening of the alignment. If we choose  $n$  even larger (not shown here), the memory (as mentioned, in the discussion of Fig. 1) disappears completely, and there is no ordering or alignment at all.

The main conclusion at this point is that there is an optimal value for the capping layer thickness, to obtain best ordering. For the system discussed here, it is  $n = 2$ . The optimal thickness depends on size, height and shape of island but is nearly independent of the misfit. We believe that such an optimal thickness exists for all strained systems and we suggest that exploring this pa-

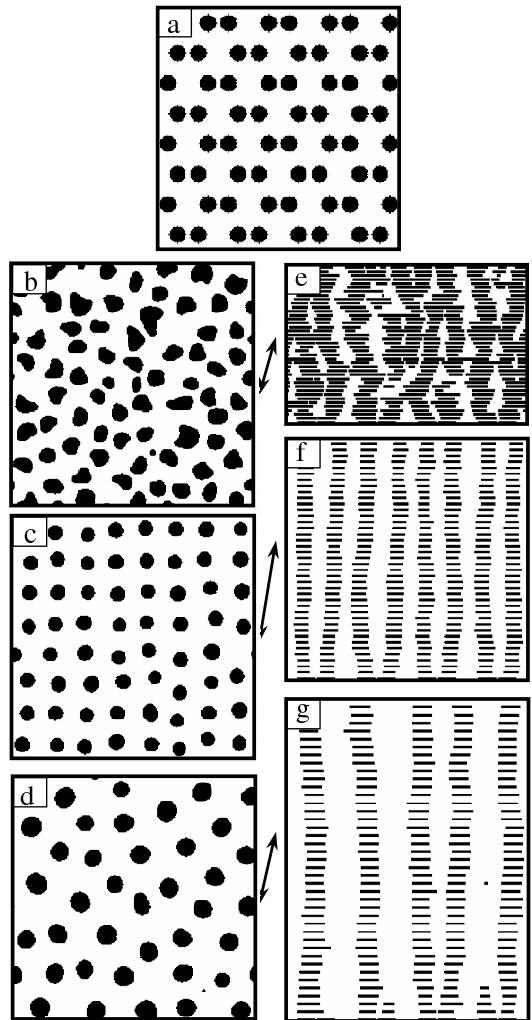


FIG. 2: Top views ((b),(c),(d)) and side views ((e),(f),(g)) of the morphologies obtained with different capping layer thickness  $n = 0$  ((b), (e)),  $n = 2$  ((c), (f)) and  $n = 4$  ((d), (g)) for  $N = 40$ . Also shown is the initial pattern (a).

rameter will guide experimentalists toward better ordering of stacked QDs. Note that Fig. 1 suggests a larger optimal thickness. The reason is that we chose a larger island in that case, to see a better transition.

The artificial patterning discussed above will of course be difficult to realize experimentally. But in the following we will show that an optimal thickness is also present for a more realistic case. We consider a system with an initially constant PES. i.e., there is initially no thermodynamic drift, and diffusion is spatially constant. A typical morphology grown in such a case is shown in Fig. 3(a). There is no ordering, and the island size distribution (ISD) is rather broad (cf. Fig. 4). We repeat the same procedure as above: We add a perfectly flat capping layer of thickness  $n$ , solve the elastic equations, and then grow a new set of islands that nucleate and grow according to the PES that has been modified due to the strain. This is repeated for  $N = 40$  superlayers. We find

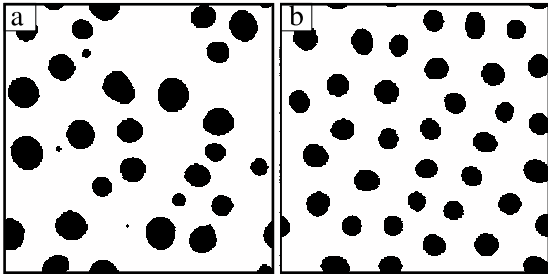


FIG. 3: Top view of the initial morphology grown on fully relaxed substrate (a) and QDs pattern with  $n = 2$  capping layers after  $N = 20$  super layers have been grown (b).

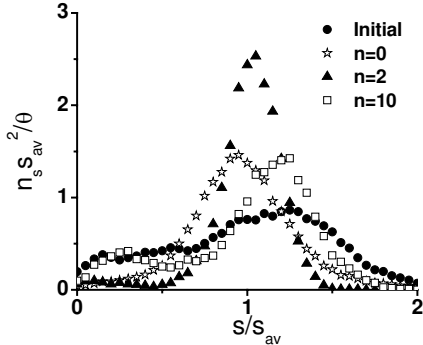


FIG. 4: Scaled island size distributions with different capping layer thickness ( $n = 0, 2$  and  $10$ ) for initial morphology and  $N = 40$ .  $n_s$  is the density of islands of size  $s$ ,  $s_{av}$  is the average island size, and  $\Theta$  is the coverage. The results represent averages over at least 40 independent simulations on a lattice of size  $200 \times 200$ . The initial morphology and  $n = 2$  correspond to the top views in Fig. 3.

that there is an optimal thickness  $n = 2$  for the capping layer. A snapshot of the morphology after  $N = 40$  superlayers have been grown is shown in Fig. 3(b). Clearly, the island arrangement and size distribution is very regular. This can also be seen by looking at ISD [c.f. Fig. 4], which is extremely narrow with a high peak. For smaller or larger values of  $n$ , ordering is not as good, as it is evident from the remaining curves in Fig. 4. Our results therefore suggest that ordering of stacked quantum dots can be improved in experiments by optimizing the thickness of the buffer layer, which could have significant impact on devices and their applications.

Our results might provide a pathway to other novel structures such as quantum dot molecules [27], or stacks of anti-aligned dots [28]. For example, Fig. 5(a) shows a top view of the anti-alignment of superlayers  $N=10$  and  $N=11$ , where the dots have grown with very thin capping layers. We get similar results for all pairs of subsequent superlayers. This anti-alignment is also evident from a comparison of the island-island correlation functions between islands in layer 10 (Fig. 5(b)), and between islands in layers 10 and 11 (Fig. 5(c)). In Fig. 5(b), the first peak is at  $\sim 15.5$ , which corresponds to the typical is-

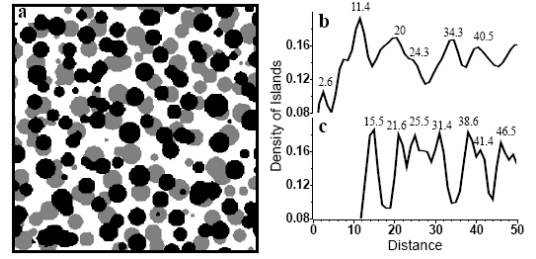


FIG. 5: Top view of anti-aligned quantum dots with a thin capping layer ( $n=0$ ) for  $N=10$  (grey) and  $N=11$  (black) (a), island-island correlation between islands within layer 10 (b), and between layers 10 and 11 (c). In (b) the positions 15.5, 21.6, 31.4, 41.4, and 46.5 correspond to the unit length multiplied by  $1, \sqrt{2}, 2, 2\sqrt{2}$ , and  $3$ . In (c) the peak positions 11.4 and 34.3 correspond to  $1/\sqrt{2}$  and  $3/\sqrt{2}$ . All of these numbers are consistent with an ideal square lattice. The remaining peaks can be reconciled with a hexagonal lattice.

land separation in layer 10. In Fig. 5(c), the first peak is at 11.4, which is  $\sim 15.5/\sqrt{2}$ , that corresponds to the center site in a square lattice. We note that such anti-alignment has been shown in a recent paper [28] that was published after our initial submission of this manuscript.

This research was supported in part by the MARCO Center on Functional Engineered NanoArchitectonics (FENA) and by the NSF through grants DMS-0402276 and DMS-0439872.

- 
- [1] S. Fafard et al., *Science* **274**, 1350 (1996).
  - [2] Shoji H et al., *Appl. Phys. Lett.* **71**, 193 (1997).
  - [3] S. Sun, C.B. Murray, D. Weller, L. Folks, and A. Moser, *Science* **287**, 1989 (2000).
  - [4] M. Valden, X. Lai, and D.W. Goodman, *Science* **281**, 1647 (1998).
  - [5] V.A. Shchukin and D. Bimberg, *Rev. Mod. Phys.* **71**, 1125 (1999).
  - [6] J. Stangl, V. Holy, and G. Bauer, *Rev. Mod. Phys.* **76**, 725 (2004).
  - [7] D.J. Eaglesham and M. Cerullo, *Phys. Rev. Lett.* **64**, 1943 (1990).
  - [8] Y.-W. Mo, D.E. Savage, B.S. Swartzentruber, and M.G. Lagally, *Phys. Rev. Lett.* **65**, 1020 (1990).
  - [9] S. Guha, A. Madhukar, and K.C. Rajkumar, *Appl. Phys. Lett.* **57**, 2110 (1990).
  - [10] C. Teichert, M.G. Lagally, L.J. Peticolas, J.C. Bean, and J. Tersoff, *Phys. Rev. B* **53**, 16334 (1996).
  - [11] Q. Xie, A. Madhukar, P. Chen, and N.P. Kobayashi, *Phys. Rev. Lett.* **75**, 2542 (1995).
  - [12] B. Lita, R.S. Goldman, J.D. Phillips, and P.K. Bhat-tacharya, *Appl. Phys. Lett.* **74**, 2824 (1999).
  - [13] J. Tersoff, C. Teichert, and M.G. Lagally, *Phys. Rev. Lett.* **76**, 1675 (1996).
  - [14] B. Yang, F. Liu, M.G. Lagally, *Phys. Rev. Lett.* **92**, 025502 (2004).
  - [15] S.M. Wise et al., *Appl. Phys. Lett.* **87** 133102 (2005).

- [16] M. Petersen, C. Ratsch, R.E. Caffisch, and A. Zangwill, Phys. Rev. E **64**, 061602 (2001).
- [17] C. Ratsch et al., Phys. Rev. B **65**, 19503 (2002).
- [18] X. Niu, R. Vardavas, R. E. Caffisch, and C. Ratsch, Phys. Rev. B **74**, 193403 (2006)
- [19] R.E. Caffisch, W. E, M.F. Gyure, B. Merriman, and C. Ratsch, Phys. Rev. E. **59**, 6879 (1999).
- [20] J. Venable, Philos. Mag. **27**, 697 (1973); G.S. Bales and D.C. Chrzan, Phys. Rev. B **50**, 6057 (1994).
- [21] A.C. Schindler et al., Phys. Rev. B **67**, 075316 (2003).
- [22] E. Penev, P. Kratzer, and M. Scheffler, Phys. Rev. B **64**, 085401 (2001).
- [23] C. Ratsch, A.P. Seitsonen, and M. Scheffler, Phys. Rev. B **55**, 6750 (1997).
- [24] C. Ratsch, Phys. Rev. B **63**, 161306(R) (2001).
- [25] C. Wöll, S. Chiang, R.J. Wilson, and P.H. Lippel, Phys. Rev. B **39**, 7988 (1989).
- [26] J. He, H. J. Krenner, C. Pryor, J. P. Zhang, Y. Wu, D. G. Allen, C. M. Morris, M. S. Sherwin, and P.M. Petroff, Nano Lett. **7(3)**, 802 (2007).
- [27] Z.M. Wang, K. Holmes, Y.I. Mazur, K.A. Ramsey, and G.J. Salamo, Nanoscale Res. Lett., 1:57 (2006).
- [28] A. Lévesque, N. Shtinkov, R.A. Masut, and P. Desjardins, Phys. Rev. Lett. **100**, 046101 (2008).